# Dynamic Distribution of Cells in Porous Scaffolds During Cell Loading

Qianqian Han[1] Chao Li[1] Haifeng Liu[2] Boon Chin Heng[3] Gang Wu[4]

Zigang Ge[1,5,*]

[1]Department of Biomedical Engineering, College of Engineering, Peking University, Beijing 100871, China
[2]School of Biological Science and Medical Engineering, School of Biological Science and Medical Engineering, Beijing 100191, China
[3]Department of Biosystems Science and Engineering, ETH-Zurich, Mattenstrasse 26, Basel 4058, Switzerland
[4]School of Material Science and Engineering, South China University of Technology, Guangzhou 510640, China
[5]Center for Biomedical Materials and Tissue Engineering, Academy for Advanced Interdisciplinary Studies, Peking University, Beijing 100871, China

Received 30 Jan 2013; Accepted 16 Apr 2013; doi: 10.5405/jmbe.1445

**Abstract**

Little is known about the cell loading process, as the majority of tissue engineering studies focus on relatively long time points. The present study investigates the dynamic distribution of cells during the initial cell loading process in porous scaffolds, namely those made of type-I collagen and silk fibroin, with similar porosities and pore sizes. Loading efficiency of the cells was higher in the silk fibroin scaffold (90%±1.8%) compared to that in the type-I collagen scaffold (76%±1.0%). There were significantly more unattached cells in the type-I collagen scaffold at 0.5 h compared to those in the silk scaffold ($p$ = 0.03). The number of adherent cells decreased with time in the type-I collagen scaffold ($p$ = 0.01), whereas in the silk scaffold, the loading cells gradually attached to the biomaterials or aggregated with time. The majority of the cells gradually attached to the scaffolds within 6 h and exhibited an elongated morphology, which did not change. In general, there was no significant difference in cell adhesion and cell morphology between the two types of scaffold. The initial six hours were critical for the cell seeding process.

***Keywords***: Chondrocytes, Cell loading, Scaffolds, Tissue engineering

## 1. Introduction

A lot of progress has been made in tissue engineering, such as that in tissue/organ regeneration, the development of tissue engineering research models, and drug delivery [1]. Tissue-engineered bladders have been demonstrated to function well in human bodies [2,3], and tissue-engineered trachea have been used to reset dysfunctional airways [4]. Autologous chondrocyte implantation (ACI) and matrix-enhanced ACI have been used to regenerate hyaline cartilage [5]. Pre-shaped scaffolds loaded with growth factors can effectively reconstruct a whole articular surface [3]. Seed cells and scaffold biomaterials are essential components during these processes. Biomaterials provide bioactive signals as well as structural support and guidance. Cells play a critical role in regeneration, regardless of whether they are loaded *in vitro* or recruited *in vivo* into the scaffolds. Therefore, cell-scaffold interaction is particularly important for the subsequent functionality of tissue-engineered constructs.

Various techniques have been used to optimize cell seeding efficiency, such as filtration, perfusion, and centrifugation [6]. Both biological adhesion factors and magnetic nanoparticles have been immobilized on scaffolds to improve cell-matrix interaction [7]. The distribution of cells on scaffold biomaterials and subsequent cell aggregation and attachment significantly influence the cell phenotype [8,9]. Previous studies have aimed to improve loading efficiency and achieve a homogeneous distribution after cell loading [10,11]. Individual cells may encounter different microenvironments, consequently leading to different cell fates. While some cells may undergo apoptosis due to mechanical injury, some may adhere to other cells instead of scaffold materials [12]. It is unclear what happens to the cells during the initial cell loading process and how cells respond to the new environment immediately after cell loading.

Material properties, including composition, porosity, pore size, and surface roughness, and mechanical properties affect the distribution, adhesion, and morphology of the cells, and thus affect the cell phenotype [13]. Natural scaffold compositions with a recognition motif for adhesion receptors, such as arginine-glycine-aspartic acid (RGD), on the surface enhance

* Corresponding author: Zigang Ge
Tel: +86-10-62756736; Fax: +86-10-62757545
E-mail: gez@pku.edu.cn

cell adhesion [14]. Although a porosity of 90% and a pore size of larger than 100 μm have been broadly adopted, scaffolds with a broad range of porosities, pore sizes, and homogeneity have been used, making the acquired results incomparable in most cases [15,16]. The topography of scaffolds may affect cell shape and distribution after seeding [9]. Scaffolds with nanofibers can maintain the differentiated phenotype of chondrocytes by hampering the formation of elongated cells, while large fibers (above 10 μm, the diameter of spherical chondrocytes) fail to maintain the chondrocyte differentiated state [9,13]. Stiff scaffolds hinder cell proliferation and migration while facilitating cell attachment [17].

The present study designed collagen and silk fibroin scaffolds with a porosity of about 90% and a pore size of approximately 150 μm to investigate the dynamic distribution and behavior of chondrocytes during the initial loading process [15,16]. Collagen and silk fibroin were chosen due to their biocompatibility, ease of fabrication, and wide use in tissue engineering [5]. The dynamic attachment, distribution, morphology, and aggregation of chondrocytes in the scaffold biomaterials were evaluated after several hours with fluorescence labeling and confocal microscopy with image analysis (Fig. 1).

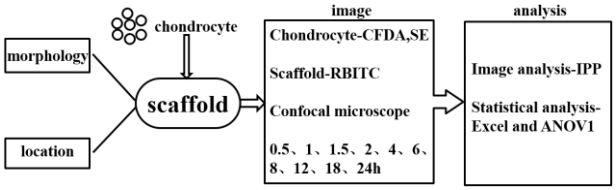


Figure 1. Flow chart of cell loading process.

## 2. Materials and methods

### *2.1 Fabrication and characterization of scaffolds*

Raw *Bombyx mori* silk fibers were purchased from Suzhou Maoda Textile Co. Ltd (Suzhou City, Jiangsu Province, China). Silk fibroin solution was obtained from raw silk fibers that were degummed in a 0.1% (w/v) $Na_2CO_3$ solution, dissolved in $CaCl_2$-$CH_3CH_2OH$-$H_2O$ (molar ratio = 1:2:8) at 78 ± 2 ℃ with continuous stirring, and subsequently dialyzed against distilled water using SnakeSkin pleated dialysis tubing (Pierce, MW cut-off: 3500 kDa). The silk fibroin solution was freeze-dried for 36 h to form a silk fibroin scaffold. After the silk fibroin scaffolds were immersed in 100% methanol for 10 min, they were dried overnight in a fume hood and stored in a vacuum- drying desiccator until use.

The collagen solution (4 mg/ml, Qi Sheng Biotechnology Co. Ltd., Shanghai, China) was poured into a plastic mold, whose diameter and height were both 10 mm, and subsequently frozen at -60 ℃ for 4 h and lyophilized for 24 h (Alpha 2-4, Christ, Germany) in a freeze-dryer to obtain a porous scaffold. The porous scaffold was cross-linked with glutaraldehyde solution (0.01%, Wt/V, Sigma, USA) for 30 min and then neutralized with glycine solution (1 mg/ml, Sigma). The scaffold was then washed three times with deionized water and lyophilized for 24 h to obtain the final porous scaffold.

The scaffolds were sectioned with a lancet and coated with gold for 80 s at 18 mA (SBC-12, KYKY Technology Co., Ltd., Beijing, China). The surface and cross-section morphology of the scaffolds were examined by scanning electron microscopy (SEM; Quanta 200FEG, FEI) at an accelerating voltage of 5 kV. To determine the mean pore size of the scaffolds, five pores in the SEM images of each scaffold were selected randomly and measured with a ruler. The maximum and minimum diameters of the pores were measured, and the average was taken as the mean pore size. In order to estimate the porosity of the two types of scaffold, the exact sizes of the scaffolds were measured with a vernier caliper and the mass of the scaffolds was carefully measured. The scaffolds were immersed in absolute alcohol for 1 h before being weighed again. Porosity was calculated as $(Ws - Wd)/(\rho/V)$, where Ws is the weight of the scaffold after immersion in absolute alcohol, Wd is the weight of the dry scaffold, ρ is the density of alcohol, and V is the volume of the scaffold [18].

### *2.2 Fluorescence labeling of scaffolds*

The type-I collagen and silk fibroin porous scaffolds were both fluorescence-labeled with isothiocyanate rhodamine B (RBITC, Sigma R1755). Before fluorescence staining, both scaffolds were cut into 3 mm × 3 mm × 1 mm samples and sterilized in 70% ethanol aqueous solution for 2 h and then under ultraviolet light for 30 min. Then, the scaffolds were immersed in 0.1 mg/ml RBITC solution for 24 h at 4 ℃. The RBITC-labeled scaffolds were then rinsed with deionized water for 24 h at 4 ℃ to remove free RBITC and finally dried under vacuum for another 24 h at 30 ℃. To prevent fluorescence quenching, the entire procedure was carried out in a dark environment. Both scaffolds had a maximum emission wavelength of ~580 nm arising from the RBITC group (excitation wavelength was 543 nm) [19].

### *2.3 Chondrocyte culture and two-dimensional observation*

The chondrocyte cell line (C28-I2) was cultured in Dulbecco's Modified Eagle Medium (DMEM/F12, Gibco) containing 10% fetal bovine serum (FBS), 100 IU/ml penicillin, and 100 μg/ml streptomycin (Gibco) within a 5% $CO_2$ incubator at 37 ℃. The seeding density was 20,000 cells per $cm^2$. The culture media were refreshed every 2-3 days.

Cells were seeded in a culture dish (100 mm × 20 mm, Corning 430167) at a density of 20,000 cells per $cm^2$. The cellular morphology was observed and imaged under light microscopy (Olympus CKX41-RC). Six time points (0 h, 15 min, 0.5 h, 1 h, 1.5 h, and 2 h) were selected to compare the maximum diameter (*dmax*) and the minimum diameter (*dmin*) of the cells in each image.

### *2.4 Fluorescence labeling of chondrocytes with CFDA-SE*

5(6)-Carboxyfluorescein diacetate N-succinimidyl ester (CFDA-SE) (-Sigma 21888) was dissolved in dimethyl sulfoxide (DMSO) (Sigma) at a concentration of 1 mM. This original stock solution was further diluted with phosphate-

buffered saline (PBS). The chondrocyte suspension was exposed to 1-5 μM CFDA-SE within a 5% $CO_2$ incubator at 37 ℃ for 20 min. The cells were then rinsed twice in PBS and resuspended in DMEM/F12. The labeled cells had an emission wavelength of 530 nm at an excitation wavelength of 490 nm [20].

*2.5 Cell loading*

The RBITC-labeled scaffolds were first rinsed and immersed in PBS for 30 min. Chondrocytes ($2 \times 10^5$ cells/scaffold) were loaded onto scaffolds in 32 wells and then cultured at 37 ℃ in 5% $CO_2$. 1 ml of DMEM/F12 was added into each well for 2 h.

*2.6 Cell seeding efficiency*

Some scaffolds were used to analyze the cell seeding efficiency. Scaffolds were kept for 0.5, 6, and 12 h under static conditions following cell seeding (n = 3). The final time point of 12 h was chosen to ensure that cells had enough time to attach and adapt to the scaffold architecture with minimal cell proliferation. At each chosen time point of culture, the cells remaining in the plates were counted using a blood cell counting chamber. Cell seeding efficiency was then calculated as:

Cell seeding efficiency = (1-number of cells remaining in plate/ cell seeding number) × 100% (1)

*2.7 Confocal laser scanning microscopy*

Ten time points, namely 0.5, 1, 1.5, 2, 4, 6, 8, 12, 18, and 24 h, were chosen for confocal microscopy observation in both the type-I collagen and silk fibroin porous scaffolds (n = 3) in this study. Cell-scaffold composites were observed under confocal microscopy (TCS-SP, Leica, Germany) with excitation wavelengths of 488 and 543 nm and emission wavelengths of 518 nm and 580 nm.

*2.8 Image analysis*

Image-Pro Plus 6.0 (IPP6.0, MediaCybernetics, America) was used to calculate the cell number and determine *dmax* and *dmin* of the cells in each image. Each single green fluorescence point was regarded as a cell. *dmax* and *dmin* were obtained by measuring the diameter of each cell. *dmax*/*dmin* is a key parameter of cell morphology and adhesion. The larger the value of *dmax*/*dmin* is, the better the cell adheres. The number of cells was also counted.

*2.9 Statistical analyse*s

Three independent images were captured (N = 3) for each scaffold at every time point, with a total of 10 time points for each scaffold. *dmax*/*dmin* values and cell numbers were subjected to statistical analysis. One-way and two-factor analyses of variance (ANOVA) were carried out. Differences between the experimental groups were considered statistically significant when $p < 0.05$.

## 3. Results

*3.1 Characterization of scaffolds*

The silk fibroin and type-I collagen scaffolds were both three-dimensional porous structures with pore sizes of approximately 150 μm (silk fibroin: 137.6 ± 18.0 μm; type-I collagen: 162.2 ± 44.4 μm). Both had a porosity of roughly 90% (silk fibroin: 87.8 ± 0.6%; type-I collagen: 87.6 ± 0.4%) with an interconnected pore structure (Fig. 2).

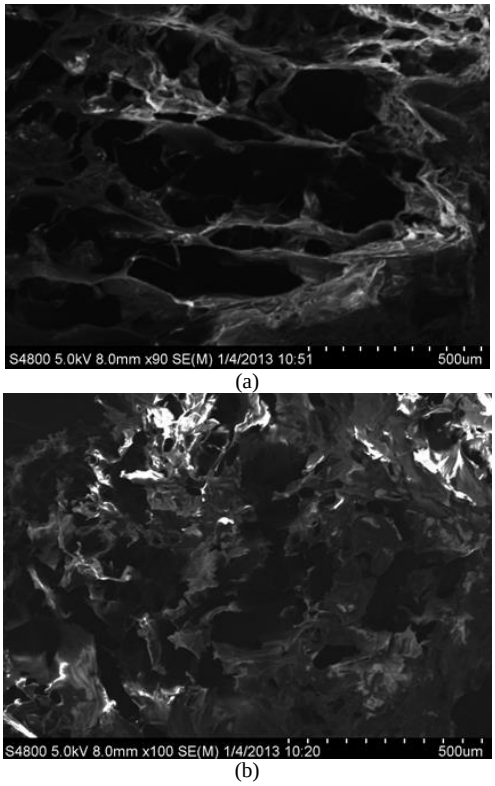


Figure 2. SEM images of surfaces of (a) type-I collagen and (b) silk fibroin scaffolds. Scale bar = 500 μm.

*3.2 Loading efficiency*

The loading efficiency of the cells within the collagen scaffold was significantly lower ($p < 0.01$) than that within the silk scaffold at all three time points (Fig. 3). There was a significant reduction ($p < 0.05$) in the cell loading efficiency of both types of scaffold from 0.5 to 6 h, with many more cells dropping from the type-I collagen scaffold onto the plate (24.4% ± 2.1%), as compared to those from the silk fibroin scaffold (9.4% ± 3.5%). Few cells were found on the culture plate with the silk fibroin scaffold, whereas many cells ($1.6 \times 10^4$ cells/well) were found in the well incubated with the type-I collagen scaffold at 0.5 h. At 6 h, only 77.8% of cells remained in the type-I collagen scaffold. The loading efficiency was as high as 92% in the silk fibroin scaffold. The final seeding efficiency at 12 h was 90.6% for the silk fibroin scaffold and only 75.6% for the type-I collagen scaffold. There was no significant difference ($p > 0.05$) between loading efficiencies at 6 and 12 h. Thus, it can be deduced that cell adhesion was stable 6 h after seeding.

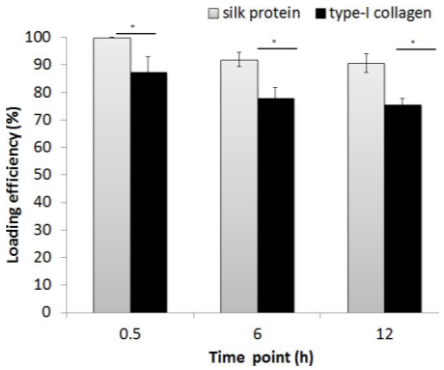


Figure 3. Chondrocytes loading efficiency at various time points. Cell number decreased on both scaffolds with time. Loading efficiency in silk protein sponge was much higher than in type-I collagen. Data are presented as mean ± standard deviation (n = 3, *$p < 0.05$ for different scaffolds compared at a given time point).

### *3.3 Cell morphology and distribution*

Cell morphology in the two-dimensional culture was observed. The *dmax*/*dmin* ratios at six time points were measured with IPP6.0 (Fig. 4). As time progressed, cells adhered to culture dishes and their *dmax*/*dmin* ratios increased. Thus, the *dmax*/*dmin* ratio is an indicator of cell adhesion.

Cell numbers in both the silk fibroin and type-I collagen scaffolds decreased with time. Both scaffolds were filled with cells 2 h after cell seeding. Cells then started to get close and adhered to the scaffolds at 4 h. Nearly all cells adhered to the scaffolds 8 h after cell seeding. The cell morphology changed; the number of round cells decreased, whereas the number of multilateral cells increased. Little round cells were observed at 8 h. The changes in the cell morphology and distribution in the two types of scaffold were the same after cell seeding. 6 h was a key time point for both scaffolds (Fig. 5).

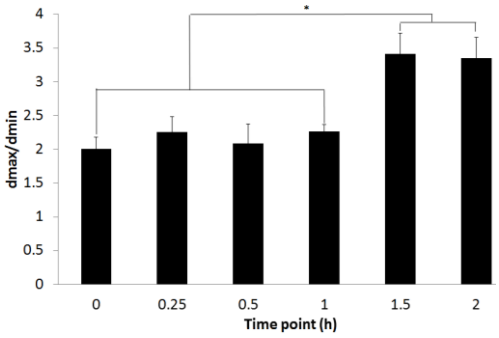


Figure 4. *dmax*/*dmin* values at each time point of two-dimensional culture. The six time points can be divided into two groups: before 1.5 h and after 1.5 h. *dmax*/*dmin* values in the after-1.5-h group increased significantly ($p < 0.05$) compared to those in the before-1.5-h group. Before 1.5 h, the average *dmax*/*dmin* was less than 2.5, and after 1.5 h, it was more than 3.0.

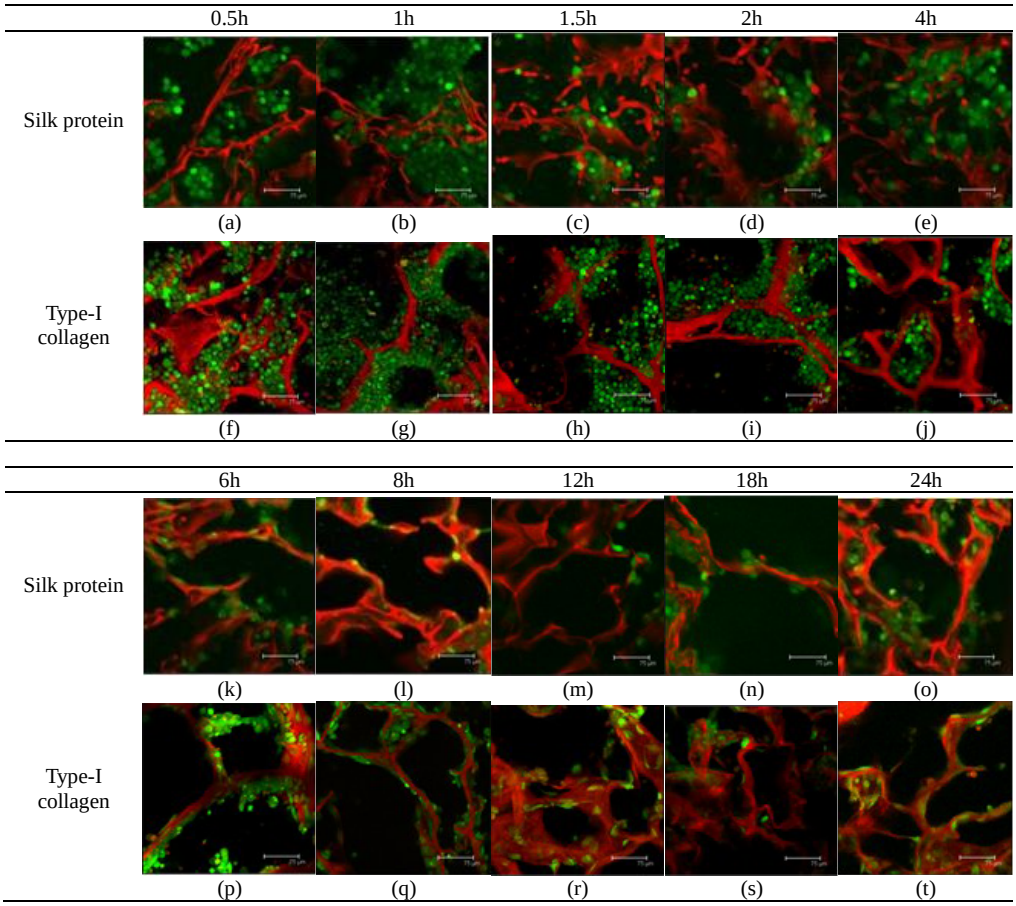


Figure 5. Chondrocyte morphology and distribution at 24 h. Cells (green) adhered to scaffold surface (red) with time. The changes in cell distribution in the two types of scaffold were nearly the same. Scale bar = 75 μm. (a-j) Chondrocytes in silk fibroin scaffold. (k-t) Chondrocytes in type-I collagen scaffold.

### 3.4 Numbers of chondrocytes in scaffolds

The trend in the variation of cell numbers during the initial cell loading process was analyzed by confocal microscopy imaging with IPP6.0 (Fig. 6). The cell number after seeding was compared to the initial cell number. The number of cells decreased in the type-I collagen scaffold; nearly 35% of the initial cells were observed in the image at 24 h. However, since the cell loading efficiency was 76%, the actual number of cells adhered to the scaffold was much higher, as many were hidden behind the type-I collagen fibers. For the silk fibroin scaffold, the cell number did not change much with time; it slightly decreased at 24 h.

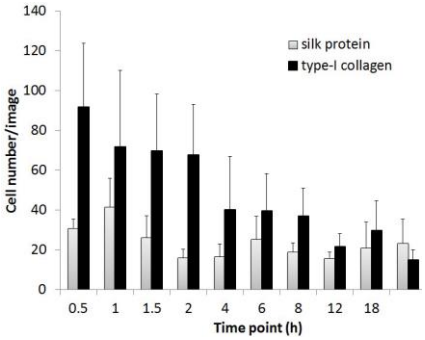


Figure 6. Cell numbers in every image of silk fibroin and type-I collagen scaffolds. Cell numbers decreased gradually in type-I collagen I scaffold, with only nearly 35% of cells remaining 24 h after seeding. In silk fibroin scaffold, cell number decreased, but did not have a significant trend.

The initial cell number obtained from the confocal images of the type-I collagen scaffold was much higher than obtained for the silk fibroin scaffold, which contradicts the measured values of cell loading efficiency. This discrepancy may be due to the small difference in pore size (silk fibroin: 137.6 ± 18.0 μm, type-I collagen: 162.2 ± 44.4 μm) between the two scaffolds. More cells were retained within the silk fibroin scaffold due to its smaller pore size. But cells had to adhere onto different surfaces and their fluorescence was hidden behind the scaffold fiber. As a result, even with a higher loading efficiency in silk scaffold, cell number obtained from the confocal images was lower. In a single image, it was difficult to detect all the cells. The larger pore size of the type-I collagen scaffold led to its lower loading efficiency.

In our study, cell numbers in both scaffolds decreased with time. Some cells dropped on the plate and thus the loading efficiency was less than 100%. Moreover, because cells adhered to the scaffold, it was impossible to view all the cells by confocal microscopy. After cell adhesion, many chondrocytes were hidden beneath the surface of the type-I collagen scaffold, which led to a decrease in the observed cell number. In contrast, the silk fibroin scaffold comprised fibers with a smaller diameter, and thus most cells in it were observable in a confocal image, so the cell numbers at different time points were more stable.

### 3.5 Cell Adhesion

The morphology of the chondrocytes changed as they adhered to the scaffolds. Upon adhesion, they cannot remain round. Multilateral cells have larger *dmax*/*dmin* values than those of round ones. According to the statistical data from confocal images, there was no difference in the cells' *dmax*/*dmin* ratio between the two types of scaffold ($p = 0.84$). *dmax*/*dmin* increased significantly ($p < 0.05$) with time (Fig. 7). Hence, time has a greater effect than scaffold material on the cellular adhesion process.

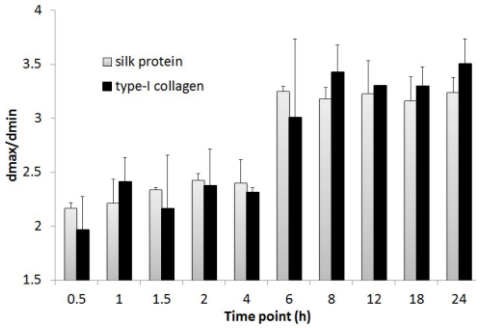


Figure 7. *dmax*/*dmin* values at every time point for the two types of scaffold. No significant difference ($p > 0.05$) was found between the two scaffolds. 6 h is a key time point. The ten time point can be divided into two groups: before 6 h and after 6 h. In each scaffold, *dmax*/*dmin* in the after-6-h group increased significantly ($p < 0.05$) compared to that in the before-6-h group. Before 6 h, the average *dmax*/*dmin* value was less than 2.5, and after 6 h, it was more than 3.0.

In both silk fibroin and type-I collagen scaffolds, the *dmax*/*dmin* values of cells did not increase significantly ($p > 0.05$) within the first 6 h. There was also no significant difference ($p > 0.05$) between cell numbers from 6 to 24 h. However, the *dmax*/*dmin* values of each scaffold at time points 0-4 h and 6-24 h were significantly different ($p < 0.01$). Before 6 h, the average value of *dmax*/*dmin* was less than 2.5, and after 6 h, it was more than 3.0. Thus, 6 h is a key time point for chondrocyte adhesion on both types of scaffold. The statistical data are consistent with the imaging results that all cells with a *dmax*/*dmin* value larger than 3.0 were polygons. According to the above results, the threshold value of a cell's *dmax*/*dmin* is 3.0. There was an upsurge of polygonal cells 6 h after cell seeding (Fig. 8).

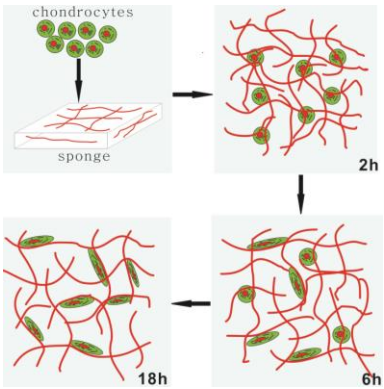


Figure 8. Schematic drawing of cell loading process in two types of scaffold after seeding. Before 6 h, cells were spherical and dispersed wildly in the sponge, without cell-cell or cell-matrix adhesion. After 6 h, chondrocytes adhered to scaffold fibers and extended into polygonal cells.

## 4. Discussion

Both cell type and cell loading density significantly affect the cell loading process. Integrin-mediated cell adhesion is involved in the cellular response to environmental stimuli [21]. Integrins also modulate cellular physiology by transmitting external mechanical stimuli into the cells [22]. An integrin can bind to its cognate ligand in the extracellular matrix (ECM) molecules only after it is activated through G-protein-coupled receptors on the cell membrane. Many factors are involved in this complex process, including the composition of biomaterials, GTPases, and enzymes such as kinases, phosphatases, proteases, and lipases [23,24]. The activities and densities of integrins vary with cell type, so it takes different times for different cells to attach and spread upon a given micro-environment. For example, pre-osteoplastic cells spread on a type-I collagen scaffold after 26 min [7], whereas rat Schwann cells start extension on type-I collagen after 16-24 h [11]. Additionally, cell seeding density may be a crucial factor in the cell loading process. The tyrosine phosphorylation level and activity of focal adhesion kinase (FAK) gradually declines with increasing cell density, which may be responsible for observed changes in cell proliferation, adhesion, and migration [25].

It took cells similar times to attach onto the two types of scaffold [25]. It has been reported that the initial cell attachment of fibroblast cells in silk fibroin is the same as that of those in type-I collagen, as determined by comparing cell morphology and growth in the two scaffolds at different time points, though the cells attached to the two scaffolds via different mechanisms [26]. The electrostatic interactions between the cells and the amino acid residues of silk fibroin promote cell-fibroin attachment. As animal cells have a predominantly negative charge on their surface, cell attachment to the silk fibroin scaffold probably results from the presence of positively charged residues such as arginine near the C-terminus of non-repetitive regions of the amino acid sequence [26,27]. The binding of integrins to glycoproteins mediates cell adhesion to type-I collagen, whereas fibronectin as well as vitronectin and laminin link collagen fibrils to the short α5β1 integrin recognition motif RGD [28]. $\alpha_1\beta_1$ and $\alpha_2\beta_1$ integrins are known to be specific type-I collagen receptors. The binding of $\alpha_1\beta_1$ and $\alpha_2\beta_1$ to collagens is divalent-cation-dependent; these integrins are promoted by magnesium and manganese but inhibited by calcium. The recognition motif of both these integrin isoforms on type-I collagen is Gly-Phe-Hyp-Gly-Glu-Arg (GFOGER), which is different from the α5β1 integrin recognition motif RGD [29,30]. Because cells need time to respond via macromolecules, this may explain the lower loading efficiency in the type-I collagen scaffold after 0.5 h.

Cell adhesion comprises cell-matrix binding, cell spreading, and the formation of focal adhesions and stress fibers [24]. Our results show comparable cell-matrix attachments and cell spreading in silk fibroin and collagen scaffolds. Further study of the formation of focal adhesions and stress fibers is needed. As the ratio *dmax*/*dmin* cannot clearly distinguish cell-cell and cell-matrix contact, fluorescence staining of integrins, cadherins, the cytoskeleton, and the cell membrane should be utilized to detect the formation of focal adhesions and stress fibers. Different cells and scaffolds with various composition and structures should be studied.

## 5. Conclusion

The dynamic distribution of cells during the initial cell loading process in type-I collagen and silk fibroin scaffolds was investigated. The majority of chondrocytes either attached onto the scaffolds or aggregated into cell clusters within 6 h after loading. The composition of the scaffold did not significantly affect the dynamics of cell attachment.

## Acknowledgements

The authors acknowledge the support from the National Basic Research Program of China (973 Program) (grant 2012CB619100), as well as the National Natural Science Foundation of China (grant 81271722).

## References

[1] S. Sieh, A. A. Lubik, J. A. Clements, C. C. Nelson and D. W. Hutmacher, "Interactions between human osteoblasts and prostate cancer cells in a novel 3D in vitro model," *Organogenesis*, 6: 181-188, 2010.

[2] B. P. Kropp and J. B. Zwischenberger, "Tissue-engineered autologous bladders: new possibilities for cystoplasty," *Nat. Clin. Pract. Urol.*, 3: 588-589, 2006.

[3] Amgad M. Haleem and Constance R. Chu, "Advances in tissue engineering techniques for articular cartilage repair," *Operative Techniques in Orthopaedics*, 20: 76-89, 2010.

[4] P. Macchiarini, P. Jungebluth, T. Go, M. A. Asnaghi, L. E. Rees, T. A. Cogan, A. Dodson, J. Martorell, S. Bellini, P. P. Parnigotto, S. C. Dickinson, A. P. Hollander, S. Mantero, M. T. Conconi and M. A. Birchall, "Clinical transplantation of a tissue-engineered airway," *Lancet*, 372: 2023-2030, 2008.

[5] C. Chung and J. A. Burdick, "Engineering cartilage tissue," *Adv. Drug Deliv. Rev.*, 60: 243-262, 2008.

[6] K. Shimizu, A. Ito, M. Arinobe, Y. Murase, Y. Iwata, Y. Narita, H. Kagami, M. Ueda and H. Honda, "Effective cell-seeding technique using magnetite nanoparticles and magnetic force onto decellularized blood vessels for vascular tissue engineering," *J. Biosci. Bioeng.*, 103: 472-478, 2007.

[7] A. V. Taubenberger, M. A. Woodruff, H. Bai, D. J. Muller and D. W. Hutmacher, "The effect of unlocking RGD-motifs in collagen I on pre-osteoblast adhesion and differentiation," *Biomaterials*, 31: 2827-2835, 2010.

[8] B. Wang, Y. Zhao, H. Lin, B. Chen, J. Zhang, X. Wang, W. Zhao and J. Dai, "Phenotypical analysis of adult rat olfactory ensheathing cells on 3-D collagen scaffolds," *Neurosci. Lett.*, 401: 65-70, 2006.

[9] S. N. Marlovits, C. Norbert, A. Christian, R. Heinz, V. Vilmos and Stefan, "The influence of scaffold architecture on chondrocyte distribution and behavior in matrix-associated chondrocyte transplantation grafts," *Biomaterials*, 32: 1032-1040, 2011.

[10] Y. S. Cohen, K. Olga and Smadar, "Integration of multiple cell-matrix interactions into alginate scaffolds for promoting cardiac tissue regeneration," *Biomaterials*, 32: 1838-1847, 2011.

[11] A. B. S, L. Franz, O. D. Dan, D. Ronald, B. Arne, S. Tilman, J. Christoph, V. S. Christoph, T. Rene, K. Eiji and S. Bernd, "The role of microstructured and interconnected pore channels in a collagen-based nerve guide on axonal regeneration in peripheral nerves," *Biomaterials*, 33: 1363-1375, 2012.

[12] K. M. Woo, J. Seo, R. Zhang and P. X. Ma, "Suppression of apoptosis by enhanced protein adsorption on polymer/ hydroxyapatite composite scaffolds," *Biomaterials*, 28: 2622-2630, 2007.
[13] E. M. B. Barabino, L. Gary and A. Gilda, "Enhancing cell seeding of scaffolds in tissue engineering through manipulation of hydrodynamic parameters," *J. Biotechnol.*, 129: 516-531, 2007.
[14] R. F. Loeser, "Chondrocyte integrin expression and function," *Biorheology*, 37: 109-116, 2000.
[15] M. M. C. G. Silva, L. A. Cyster, J. J. A. Barry, X. B. Yang, R. O. C. Oreffo, D. M. Grant, C. A. Scotchford, S. M. Howdle, K. M. Shakesheff and F. R. A. J. Rose, "The effect of anisotropic architecture on cell and tissue infiltration into tissue engineering scaffolds," *Biomaterials*, 27: 5909-5917, 2006.
[16] S. H. Oh, I. K. Park, J. M. Kim and J. H. Lee, "In vitro and in vivo characteristics of PCL scaffolds with pore size gradient fabricated by a centrifugation method," *Biomaterials*, 28: 1664-1671, 2007.
[17] N. Minoura, S.-I. Aiba, Y. Gotoh, M. Tsukada and Y. Imai, "Attachment and growth of cultured fibroblast cells on silk protein matrices," *J. Biomed. Mater. Res.*, 29: 1215-1221, 1995.
[18] C. Li, L. Wang, Z. Yang, G. Kim, H. Chen and Z. Ge, "A viscoelastic chitosan-modified three-dimensional porous poly(L-lactide-co-epsilon-caprolactone) scaffold for cartilage tissue engineering," *J. Biomater. Sci. Polym. Ed.*, 23: 405-424, 2012.
[19] C. Simonsson, J. T. Madsen, A. Graneli, K. E. Andersen, A. T. Karlberg, C. A. Jonsson and M. B. Ericson, "A study of the enhanced sensitizing capacity of a contact allergen in lipid vesicle formulations," *Toxicol. Appl. Pharmacol.*, 252: 221-227, 2011.
[20] X. Li, H. Dancausse, I. Grijalva, M. Oliveira and A. D. Levi, "Labeling Schwann cells with CFSE-an in vitro and in vivo study," *J. Neurosci. Methods*, 125: 83-91, 2003.
[21] K. Hozumi, D. Otagiri, Y. Yamada, A. Sasaki, C. Fujimori, Y. Wakai, T. Uchida, F. Katagiri, Y. Kikkawa and M. Nomizu, "Cell surface receptor-specific scaffold requirements for adhesion to laminin-derived peptide-chitosan membranes," *Biomaterials*, 31: 3237-3243, 2010.
[22] E. Lucchinetti, M. M. Bhargava and P. A. Torzilli, "The effect of mechanical load on integrin subunits alpha 5 and beta 1 in chondrocytes from mature and immature cartilage explants," *Cell Tissue Res.*, 315: 385-391, 2004.
[23] E. Montanez, S. Ussar, M. Schifferer, M. Bosl, R. Zent, M. Moser and R. Fassler, "Kindlin-2 controls bidirectional signaling of integrins," *Genes Dev.*, 22: 1325-1330, 2008.
[24] J. T. Parsons, A. R. Horwitz and M. A. Schwartz, "Cell adhesion: integrating cytoskeletal dynamics and cellular tension," *Nat. Rev. Mol. Cell Biol.*, 11: 633-643, 2010.
[25] F. Xu and Z. J. Zhao, "Cell density regulates tyrosine phosphorylation and localization of focal adhesion kinase," *Exp. Cell Res.*, 262: 49-58, 2001.
[26] Y. Gotoh, M. Tsukada and N. Minoura, "Effect of the chemical modification of the arginyl residue in Bombyx mori silk fibroin on the attachment and growth of fibroblast cells," *J. Biomed. Mater. Res.*, 39: 351-357, 1998.
[27] Y. Wang, H.-J. Kim, G. Vunjak-Novakovic and D. L. Kaplan, "Stem cell-based tissue engineering with silk biomaterials," *Biomaterials*, 27: 6064-6082, 2006.
[28] J. Heino, M. Huhtala, J. Käpylä and M. S. Johnson, "Evolution of collagen-based adhesion systems," *Int. J. Biochem. Cell Biol.*, 41: 341-348, 2009.
[29] J. Emsley, C. G. Knight, R. W. Farndale and M. J. Barnes, "Structure of the integrin α2β1-binding collagen peptide," *J. Mol. Biol.*, 335: 1019-1028, 2004.
[30] M. B. Rahmany and M. Van Dyke, "Biomimetic approaches to modulate cellular adhesion in biomaterials: A review," *Acta Biomater.*, 9: 5431-5437, 2013.